REPONSES OF THE JOVIAN ATOMOSPHERE TO COMETARY PARTICLES AND PHOTON IMPACTS

NAG5-4986

Annual Progress Report

for the period June 15, 1997 through June 14, 1998

Principal Investigator

Dr. A. Dalgarno

March 1998

Prepared for

National Aeronautics and Space Administration

Smithsonian Institution
Astrophysical Observatory
Cambridge, Massachusetts 02128

The Smithsonian Astrophysical Observatory
is a member of the
Harvard-Smithsonian Center for Astrophysics

The NASA Technical Officer for this grant is Dr. Jay Bergstralh, NASA/HQ
Code S, Washington, DC 20546-0001

Responses of the Jovian Atmosphere to
Cometary Particles and Photon Impacts
NAG5-4986
Progress Report

We have focused our attention on a study of the deposition of heavy ions in the Jupiter atmosphere. As discussed by Horanyi et al (1988), Waite et al. (1994) and Cravens et al. (1993), in their passage through the atmosphere the ions undergo stripping and charge transfer collisions producing excited ions which radiate in the *X*-ray and ultraviolet regions of the spectrum. Cravens (1997) has suggested that a similar mechanism is responsible for *X*-ray emission observed from comets. The previous analyses have adopted an equilibrium charge distribution approximation in which it is assumed that any energy the ratio of production and loss of a specific charge state q are equal. The distribution is then independent of the ion history. A minimum number of collisions is required to establish the equilibrium charge distribution. There occurs a bottleneck in reaching the equilibrium charge distribution, determined by the charge-changing process with the smallest cross section, and there is no unique relationship between the projectile energy and the distribution of charge states.

We have used a Monte-Carlo simulation and employed a more comprehensive set of cross section data. We have explicit predictions for the spectra generated at wavelengths corresponding to energies greater than 100eV by

oxygen ions. A preliminary version of a paper is attached.

We are continuing with a study of the ultraviolet emissions and the inclusion of sulfur ions in the precipitating flux.

References

Cravens, T.E. Comet Hyakutake *X*-ray source:; Charge transfer of solar wind heavey ions, Geophys. Res. Lett. **24**, 105, 1997.

Cravens, T.E., E. Howell, J. H. Waite Jr., and G. R. Gladstone, Auroral oxygen preciptitation at Jupiter, J. Geophys. Res. **100**, 17153, 1995.

Horanyi, M., T.E. Cravens, J. H. Waite, Jr., The precipitation of energetic heavy ions into the upper atmosphere of Jupiter, J. Geophys. Res. **93**, 7251, 1988.

Waite, J. H. Jr., F. Bagenal, F. Seward, C. Na, G.R. Gladstone, T.E. Cravens, K. C. Hurley, J. T. Clarke, R. Elsner, and S. A. Stem, ROSAT observations of the Jupiter Aurora, J. Geophys. Res. **99**, 14, 799, 1994.

X-ray and EUV Emission Spectra of Oxygen Ions Precipitating into the Jovian Atmosphere

V. Kharchenko[1], *Weihong Liu*[2] *and A. Dalgarno*[1]
[1] *Harvard-Smithsonian Center for Astrophysics*
Cambridge, MA 02138
[2] *Physics Division, Oak Ridge National Laboratory*
Oak Ridge, TN 37831

Abstract

Spectra of soft x-ray and EUV emissions of oxygen ions, precipitating into the Jovian atmosphere, are calculated, taking into account the dynamical character of the energy and charge distributions of the ions as they propagate. Monte-Carlo simulations are performed using experimental and theoretical cross sections of ion collisions with the atmospheric gases. The numbers of x-ray and EUV photons produced per precipitating oxygen ion are calculated as functions of the initial ion energy and charge. The energy and charge distribution functions are used to evaluate the intensities of characteristic x-ray and EUV spectral emission lines of oxygen ions in the Jovian aurora.

1. Introduction

The discovery of intense x-ray emission from Jovian auroras [*Metzger et al.*, 1983, *Waite et al.*, 1994] and measurements of energetic oxygen and sulfur ions [*Gehrels and Stone*, 1983] and recent observations of x-ray and extreme ultraviolet (EUV) emission from comets [*Lisse et al.*,1996] have stimulated studies of the radiation emitted by highly stripped ions [*Horanyi et al.*, 1988, *Waite et al.*, 1994, *Cravens et al.*, 1995, *Cravens*, 1997]. Models of x-ray production in Jovian auroras have been developed in analogy to those constructed to describe ion precipitation into the terrestrial atmosphere [*Rees*, 1989]. Soft x-ray and EUV photons are emitted by the excited states of highly-charged precipitating ions. The highly-charged ions are produced by stripping collisions with the atmospheric gases and the excited states are populated by electron capture in charge transfer collisions. The intensities of the soft x-ray and EUV radiation depend on the flux of precipitating ions. The spectral distribution depends on the relative abundances of the charge states of the ions which are modified by collisions as the ions traverse the atmosphere. We introduce an energy and charge distribution function $F(q, E, t)$ where q is the ion charge , E is the energy and t is the time measured from the time $t = 0$ at which the ion enters the atmosphere. The distribution function is normalized such

$$\sum_q \int dE F(q, E, t) = 1,$$

and $F(q = 0, E = 0, t = \infty) = 1$ at the end of a stopping process. Each elementary collision in the stopping process is a multichannel scattering event with probability $p(q', E'|q, E)$ of changing the ion charge q to q' and ion energy E to E'. Charge transfer, stripping and target excitation and ionization may occur during the collision. Charge transfer and stripping collisions change E and q and target excitation and ionization change E but not q. Target ionization is a major channel for highly-charged fast ions and charge transfer dominates as the ions slow down. Cross sections for stripping, electron capture and target excitation and ionization change by orders of magnitude as the projectile energy decreases to zero from initial values of several MeV. To obtain a reliable model of the precipitating ions, the energy and charge relaxation must be considered together.

A significant simplification in the calculation of the energy and charge distribution is achieved by adopting the approximation the Equilibrium Charge Distribution (ECD) [*Horanyi et al.*, 1988, *Cravens et al.*, 1995]. The ECD is obtained with the assumption that at any energy E the rates of production and loss of a specific charge state q by stripping and charge transfer are equal. Thus the ECD is a function only of the energy E and does not depend on the ion history. A minimum number of collisions is required to establish the equilibrium charge distribution given by $N \sim 1/p_{min}$, where p_{min} is the smallest of the charge-changing probabilities $p(q \pm 1, E'|q, E)$ and there occurs a bottleneck at the charge state q corresponding to the smallest stripping or charge transfer

cross section. The ECD does not account for the consequences of the bottleneck nor does it recognize that there is no unique relationship between the projectile energy and the distribution of charge states. Because of the dependence on q on the channel probabilities , there occurs a spread in the energy and charge distributions around some mean values $\{< E(t) >, < q(t) >\}$.

In this article we investigate the dynamical evolution of the energy and charged distribution of oxygen ions precipitating into the Jovian atmosphere. The available experimental and theoretical cross sections are employed in Monte-Carlo simulations of the multichannel collisions that reduce the energy and charge to zero. The differences between the Dynamical Charge Distribution (DCD) function and the ECD function are discussed. The Monte-Carlo simulations are used to calculate the total production of X-ray and EUV radiation through the stopping process, taking into account the cascading from the excited oxygen ions.

2. Stochastic Model of an Ion Flux Propagation in a Bath Gas.

The stopping of energetic ions by atmospheric gases involves multiple elastic and inelastic collisions, which alter the internal states and kinetic energies of the projectile particles and the bath gas atoms and molecules. We investigate the dynamical changes in the energy and charge distributions of projectile particles as they are slowed down in binary collisions with the dilute bath gas. We take account of the collision processes:

$$\begin{aligned} & \rightarrow \quad O^{+(q-1)} + X^*, \quad p_-(q-1, E-\delta E_-|q,E) \\ O^{+q} + X \quad & \rightarrow \quad O^{+q} + X^*, \quad p_0(q, E-\delta E_0|q,E) \\ & \rightarrow \quad O^{+(q+1)} + X^*, \quad p_+(q+1, E-\delta E_+|q,E) \end{aligned}$$

where p_- is the probability of electron-capture collisions with mean energy change $\delta E_- = \delta E_-(q,E)$, p_0 is the probability of collisional ionization or excitation of the target molecules without changes of a projectile charge, $\delta E_0 = \delta E_0(q,E)$ is the mean value of the energy transferred and p_+ is the probability of projectile stripping collisions with a mean energy loss $\delta E_+ = \delta E_+(q,E)$. X^* describes all possible final states of the bath gas molecules. For H_2 target molecules X^* includes H_2^* , $H_2^+ + e$, $H + H^+ + e$ and $H^+ + H^+ + 2e$ final states, and for He target atoms X^* includes He^*, $He^+ + e$ and $He^{+2} + 2e$. The probabilities of energy and charge transformations in a flux of oxygen ions are given by the total collision cross sections $\sigma_t(q,E)$ and channel cross sections σ_-, σ_0 and σ_+ in which the charge is decreased , unchanged or increased. Then with the total cross section defined by:

$$\sigma_t(q,E) = \sigma_-(q,E) + \sigma_0(q,E) + \sigma_+(q,E) \qquad (1)$$

the channel probabilities are given by

$$p_- = \frac{\sigma_-}{\sigma_t}; \quad p_0 = \frac{\sigma_0}{\sigma_t}, \quad p_+ = \frac{\sigma_+}{\sigma_t}. \tag{2}$$

Examples of the energy dependence of the cross sections for different channels in $O^{+q} + H_2$ collisions are shown in Fig.1 for $q = 5$. Fig.2 presents the corresponding channel probabilities p_-, p_0 and p_+ as functions of collision energy. The database for the evaluation of multi-collision stopping processes includes 25 energy-dependent cross sections $\sigma_i(q, E)$ for the H_2 bath gas. It would be extended by 2×25 additional cross sections, if collisions with the minor constituents He and H were included. To calculate the channel probabilities we have used the available experimental cross sections for charge-transfer, stripping and target ionization processes as well as theoretical models to extrapolate the experimental data to other energies [*Cocke and Montenegro*, 1996, *Greenland,* 1982, *Montenegro and Meyerhof,* 1991, *Montenegro et al.,* 1992, *Janev and Winter,* 1985, *Paneuf et al.,* 1987, *Rost,* 1997] and references in *Horanyi et al.* (1988) and *Cravens et al.* (1995). There are differences between our input cross sections and those of *Horanyi et al.* (1988) and *Cravens et al.* (1995). In particular we have used stripping cross sections in collisions of oxygen ions with hydrogen molecules and helium atoms measured by *Montenegro et al.* (1992). These stripping cross sections are several times larger than the cross sections used in earlier calculations. The maximum value of the experimental stripping cross section in $O^{+5} + H_2$ collisions is about four times larger and the maximum is reached at the projectile energy 5 MeV compared to 16 MeV. The energy dependence and the values of the stripping cross sections are important in determining the abundances of highly charged ions. The cross sections σ_+ are about of two order of magnitude less than the total cross sections and the stripping collisions create a bottleneck in establishing the ion charge distribution.

We differ also in the evaluation of the loss of projectile kinetic energy in charge transfer collisions. The energy change in charge transfer collisions includes a loss of projectile velocity due to the additional work done by a fast moving projectile nucleus during electron pick up, given by :

$$\delta E_- = I_b - < I_{q-1}(n,l) > + \frac{m_e}{M_O} E, \tag{3}$$

where M_O is the mass of oxygen nucleus, I_b is the ionization potential of the bath gas species; $< I_{q-1}(n,l) >$ is the binding energy of the transferred electron in the $O^{+(q-1)}$ ion, averaged with respect to all quantum numbers $\{n,l\}$ of the final states [*Janev and Winter,* 1985, *Ryufuku and Watanabe,* 1979]. The last term in Eq.3, $(m_e/M_O)\ E$, describes the loss of a kinetic energy of a projectile nucleus when it picks up an electron from the initially stationary gas atom or molecule. This energy loss term dominates at very high collision energies.

The propagation of oxygen ions though a bath gas may be considered as a discrete chain of charge and energy transfer collisions. As a first step in modeling the stopping process we construct a stochastic scheme for the evolution of charge and energy states of a single oxygen ion. After n collisions with bath gas molecules the energy and charge of a selected oxygen ion are

$$E(n) = E_0 - \sum_{i=1}^{i=n} \delta E_i(q_{i-1}, E_{i-1}) \tag{4}$$

$$q(n) = q_0 + \sum_{i=1}^{i=n} \Delta q_i(q_{i-1}, E_{i-1}) \tag{5}$$

where $\{\delta E_i, \Delta q_i\}$ are respectively the energy and the charge transferred by a projectile in the $i-th$ collision. These values as well as the probabilities p_-, p_+ and p_0 depend on the ion charge and the kinetic energy before the collision. The set of inelastic collisions can be described by the unique phase trajectory of the ion charge and energy states in the $\{E, q\}$ plane. The total number of distinct trajectories after n collisions is equal to 3^n and each trajectory is weighted by the probability of a particular path:

$$P(n) = \prod_{i=1}^{i=n} p_i(q_{i-1} + \Delta q_i, E_{i-1} - \delta E_i | q_{i-1}, E_{i-1}) \tag{6}$$

The probabilities for all trajectories and the energy and charge transformation rules from Eqs.4 and 5 enable the evaluation of the changing energy and charge distributions of the precipitating ions as functions of the number of collisions n or the real time t. The time calculations can be done for a specified spatial distribution of atmospheric gas by introducing a collision time t_n :

$$t_n = \sum_{i=1}^{i=n} \delta t_i(q_{i-1}, E_{i-1}) \tag{7}$$

$$\delta t_i^{-1}(q_{i-1}, E_{i-1}) = \rho(\vec{r}_i) < v_{i-1} * \sigma_t(q_{i-1}, E_{i-1}) > \tag{8}$$

where δt_i is the time interval between the $i-1$ and i-th collisions, and $\rho(\vec{r}_i)$ is the density of the bath gas for the i-th collision. The total quantum yield and the emission spectra of precipitating ions can be calculated without a knowledge of a spatial distribution of the atmospheric gas. In a dilute bath gas the typical time interval δt_c between collisions is much larger than the typical time $\tau_r(q)$ of radiative transitions of projectile ions :

$$\frac{\tau_r(q)}{\delta t_c} = \tau_r(q)\ \rho\ v\ \sigma_t \ll 1. \tag{9}$$

If the bath gas density ρ exceeds value of $10^{16} - 10^{17} cm^{-3}$, collisions of oxygen ions become strongly correlated and oxygen ions in excited electronic states undergo collisions.

The theoretical description then should include the population and radiative relaxation of electronic excited states. The inequality, given by Eq.9, is valid for the propagation of oxygen ion fluxes in the Jovian atmosphere, if we neglect the population of long lived metastable electronic states.

The stopping of energetic oxygen ions in the Jovian atmosphere may involve millions of collisions and an evaluation of the probabilities of all collision paths in $\{E, q\}$ space is not realistic. Monte Carlo simulations of multiple collisions give samples of $\{E(n), q(n)\}$ trajectories, which describe the dynamical changes of the energy and charge states in an ensemble of initially monoenergetic ions. The stochastic scheme provides statistical information about a set of the most probable $\{E(n), q(n)\}$ trajectories and yields the evolution of the energy and charge distribution function $F(q, E, n)$ in the stopping process. Examples of the evolution are shown in Fig.3, where contours of the energy and charge distribution are plotted for a thousand particle ensemble of monoenergetic oxygen ions with initial energy of 10 MeV and initial charge of unity in the interval from $n = 2 * 10^3$ to $n = 1.5 * 10^5$ collisions. The initial energy and charge distribution spreads into a propagating $\{E(n), q(n)\}$ packet tracking the most probable trajectories. Fig.4 shows the energy and charge distribution $F(q, E, n)$ of the initially monoenergetic 20 MeV ion flux after $n = 2\ 10^5$ collisions. The central point of the energy and charge distribution may be approximately characterized by a mean energy $E_{av}(n)$ and a mean charge $q_{av}(n)$

$$E_{av}(n) = \frac{\int_0^\infty dE\ E\ \sum_{q=0}^{q=8} F(q, E, n)}{\int_0^\infty dE\ \sum_{q=0}^{q=8} F(q, E, n)} \tag{10}$$

$$q_{av}(n) = \frac{\int_0^\infty dE\ \sum_{q=0}^{q=8} q\ F(q, E, n)}{\int_0^\infty dE\ \sum_{q=0}^{q=8} F(q, E, n)}\ , \tag{11}$$

with dispersions: $\delta E_{av}(n)$ and $\delta q_{av}(n)$. The dynamical evolution of the average energies and charge values are shown in Fig.5 for oxygen ions with the initial energy of 20 MeV and initial charge of unity. The parametric dependence of the mean ion charge on mean energy, $q_{av} = q_{av}(E_{av})$, gives typical trajectories of precipitating ions in the $\{E, q\}$ plane. These trajectories are depicted in Fig.6 for different initial charges equal to 3 and 8 of an ion ensemble with initial energy of 10 MeV. The trajectory in $\{E, q\}$ space of the center of an ion packet with $E_{in} = 20\ MeV$, $q_{in} = 1$ is shown by the dashed curve. For all curves depicted in Fig.6 the mean charge is changed rapidly during the first 10^3 - 10^4 collisions. Than the phase trajectories of the mean values $\{E_{av}(n), q_{av}(n)\}$ follow a universal dependence $q_{av} = q_{av}(E_{av})$, which describes the propagation of the central point of the energy and charge distributions. The relation between the average dynamical values of q and E is given approximately by

$$q_{av}(E_{av}) = 8\ tanh\Big[\ \frac{E_{av}^2}{T_s(E_{av} + T_s)}\ \Big] \tag{12}$$

where the fitting parameter $T_s = 4.8\ MeV$. Eq.12 describes well the trajectories of the center of the energy-charge packets. This curve is close to the prediction of the ECD model, shown by points in Fig.6. Nevertheless, there are significant differences between the charge abundances in the equilibrium and dynamical distributions. Information about the mean charge value is not enough to draw conclusions about the abundances of different charge states. The population of different charge states depends on the spread of the charge distribution. In the following analysis we give a detailed explanation of the differences between charge populations in the dynamical and equilibrium distributions.

The dynamical evolution of the ion charge states from an initial charge state q_{in} is described by the charge distribution function

$$G(q, q_{in}, E_{in}, n) = \int_0^{E_{in}} dE\ F(q, E, n). \tag{13}$$

The populations of the charge states for a thousand oxygen ions with an initial energy of 10 MeV and initial charges of 3 and 8 are shown in Figs.7a and b as functions of the number of collisions. The charge distribution function G and $F(q, E, n)$ depend weakly on the initial ion charge except for the initial stages of the stopping process, as was shown also in Fig.6 for the $\{E_{av}(n), q_{av}(n)\}$ values. The spread of the charge distributions is formed by the bunch of the most probable $\{E(n), q(n)\}$ trajectories.

The spread of the dynamical charge distributions differs from the prediction of the equilibrium model. The equilibrium distribution $G_{eq}(q, E)$ depends only on the particle energy E and is calculated from the detailed balance of charge-capture and stripping processes [*Horanyi et al.,* 1988 ,*Cravens et al.,* 1995]. Fig.8 shows the difference between the dynamical $G(q, q_{in}, E_{in}, n)$ and equilibrium $G_{eq}(q, E_{av}(n))$ functions at various stages of the ion stopping process, as the number of collisions increases. Differences are large in the wings of the distribution, where the ion charges are far from the mean value. At the beginning of the stopping process, the actual charge distribution has a smaller amount of highly stripped ions than the equilibrium distribution and the $G(q, E_{in}, n)$ spreads more into the area of low charged states. At the same time the oxygen ions have lost about $\sim 7\%$ of the initial energy of 10 MeV. The relaxation of the charge abundances in the ion fluxes occurs slowly because of the low probabilities of charge changing collisions compared to energy transfer collisions. The charge population does not reach equilibrium although a significant amount of energy has been lost. Even after $n = 5 * 10^4$ collisions, when a projectile particle has lost about 45% of its initial energy, the charge abundance is still different from the ECD, as shown in Fig.7. The charge population can be reproduced approximately by the ECD function only after about $n = 10^5$ collisions, when the highly stripped ions with $q = 6, 7$ and 8 have completely disappeared from the distribution and the mean particle energies has been reduced to 3.4 MeV. The similarity between the dynamical and equilibrium distributions disappears also at small energies, where electron capture processes dominate and stripping collisions produce a bottleneck in the development the charge distribution.

For the entire stopping process the abundances of highly charged ions as well as their EUV and x-ray radiations are not adequately described by the ECD model. The actual distribution does not follow adiabatically the change in the mean energy of the ions.

3. Quantum Yield for X-ray and EUV Radiations of Oxygen Ions.

The total number of photons emitted by projectile ions deposited in the atmosphere will be calculated in this section from the dynamical energy and charge distribution functions. X-ray and EUV emission originate from electronic excited states produced in electron capture collisions of highly charged ions. The populations of ion excited states in the stopping process may be calculated with the $F(E,q,n)$ functions and the electron capture cross-sections. According to Eq.9 the typical decay time of an excited state via radiative transitions is shorter than the time interval between collisions. Each process of electron capture leads to the emission of one characteristic photon in the soft x-ray or EUV spectrum. The total number of emitted photons, the quantum yield of x-ray or EUV radiation, equals the number of corresponding $q+1 \rightarrow q$ electron-capture collisions that occur during the stopping of a projectile particle. Cascade transitions redistribute the energy of initial excitation between different emission lines, the relative intensities of which are fixed by the branching ratios of radiative transitions of the q-charged ion. A detailed description of the intensities of different spectral lines will be given in the next sections.

The quantum yield $Y(q,E_{in})$ is defined as the number of resonant photons , emitted by a single projectile particle in the $q-$charge state. Although the quantum yield may depend on initial energy and initial charge, the initial q value is important only for projectile particles with small initial energies E_{in}. The abundance of highly charged ions during the slowing down is determined mostly by multiple stripping and charge-transfer collisions and the memory of the initial charge state is lost. Examples of charge evolution from different initial charges are shown in Fig.7a and b. The number of x-ray or EUV photons emitted per second from the $\{n_q,l\}$ excited state of a q-charged ion is equal to the rate of charge transfer $q+1 \rightarrow \{q,n_q,l\}$. The rate of population of $\{n_q,l\}$ states in charge transfer collisions is given by

$$R(n_q,l,t) = \int_0^\infty dE F(E,q+1,n(t))\rho(t)v\sigma(n_q,l,E) \qquad (14)$$

where $\sigma(n_q,l,E)$ is the cross section of the state-selective electron capture process, and the $n(t)$ is the number of collisions that occurred before time t. The rate of population of excited states of a q- charge ion and the rate of emission are given by

$$R(q,t) = \int_0^\infty dE F(E,q+1,n(t))\rho(t)v\sigma^*_-(q+1,E) \qquad (15)$$

where $\sigma^*_-(q+1,E) = \sum_{n_q,l} \sigma(n_q,l,E)$ is the cross sections of electron capture by the $q+1$-charge ion into all excited states of the q-charge ion. This cross section is a fraction $\xi(q+1,E)$ of the total charge transfer cross section $\sigma_-(q+1,E)$. Values of $\xi(q+1,E)$ have been obtained from data on the relative populations of selective ion states in charge-transfer collisions [*Janev and Winter*, 1985]. At intermediate collision energies the fraction of electrons captured into the ground state of highly charged ions is small and it increases only slightly at very high energies [*Ryufuku and Watanabe*, 1979, *Greenland*, 1982, *Janev and Winter*, 1985]. The total number of soft x-ray or EUV photons, radiated in a time t from a given charge state of a projectile particle, is obtained as the time integral

$$Y(q,E_{in},t) = \int_0^t dt R(q,t)$$
$$= \int_0^{E_{in}} \int_0^t dE\ \xi(q+1,E) F(q+1,E,n(t))\ \rho(t) v \sigma_- dt \qquad (16)$$

In Eq.16 $\rho(t)v\sigma_-dt$ is the number of charge-capture collisions $dn_-(t)$ that occurred within a time interval dt. The total number of collisions $dn(t) = \rho(t)v\sigma_t(q+1,E)dt$ in the time interval dt multiplied by the probability of electron-capture process gives

$$dn_-(t) = \rho v \sigma_- dt = p_-(q+1,E)\rho v \sigma_t dt = p_-(q+1,E) dn(t). \qquad (17)$$

The time integration in Eq.16 is replaced by a summation over collisions with elementary step from Eq.17: $dn(t) = 1$. The number of photons emitted by an excited ion in the q-charge state is a function of the number of collisions $n = n(t)$ occurring in time t :

$$Y(q,E_{in},n) = \sum_{i=0}^{n} \int_0^{E_{in}} dE F(q+1,E,i) \times$$
$$\xi(q+1,E)\ p_-(q, E - \delta E_- | q+1, E), \qquad (18)$$

The numbers of x-ray and EUV photons emitted by a single oxygen projectile in different q-charge states and the ion mean energy $E_{av}(n)$ are shown in Fig.9 as functions of the number of collisions. At the beginning of the stopping process the abundances of highly charged ion states are small along with the probabilities of charge transfer collisions. Few x-ray photons are emitted before $n \sim 5 * 10^4$ collisions have taken place as shown in Fig.9. At the same time the projectile kinetic energy ΔE has been reduced on the 23% of the initial energy. Energy loss causes an increase of probabilities of electron capture collisions with a simultaneous decrease in the abundances of highly charged states. Due to that the quantum yield from the $q = 7$ charge state does not increase after the $n \sim 2 * 10^5$ collisions while the $Y(q,E_{in},n)$ values for lower charges are still growing. The number of x-ray photons, emitted by a single projectile particle, is shown in Fig.10 and 11 as functions of the mean energy $E_{av}(n)$ for initial energies of 10 MeV and 100 MeV. The number of x-ray photons emitted increases smoothly with

the initial energy of the precipitating ions. A single oxygen ion with initial energy of 10 MeV produces 15 x-ray Lyman-like photons from the $q = 7$ charge state, while a projectile with the initial energy of 100 MeV produces 23 photons.

4. Spectra of the Soft X-ray and EUV Emissions of Oxygen Ions in the Jupiter Aurora.

The yield $Y(q, E_{in}, n \to \infty)$ equals the total number of electron captures into all excited $\{n_q, l\}$ states of the q-charged ions. The total energy input into electronic excitations of ion states is redistributed by cascade transitions between the short and long-wavelength parts of the spectrum. The spectral intensities of the x-ray and EUV emissions together with cascade lines from various excited levels of oxygen ions are calculated using data on selective state populations in electron capture processes and on oscillator strengths of oxygen ions [*Green et al.*, 1957, *Striganov and Sventitskii*, 1968, *Sobelman*, 1979, *Wiese at al.*, 1996, *Hoang-Binh*, 1990]. The relative population of different excited states $\{n_q, l\}$ by electron capture depends on the projectile kinetic energy. According to Figs.9 and 10, x-ray photons from the $q = 5, 6$ and 7 charge states are produced mostly in the energy interval 2 $MeV < E < 17$ MeV. At these kinetic energies the charge transfer collisions populate a large number of excited levels [*Janev and Winter*, 1985, *Greenland*, 1982]. In Figs.12 and 13 the cascade spectra originating from excited states $O^{+7}(n_q = 8)$ and $O^{+7}(n_q = 5)$ are shown for oxygen ions with an initial energy of 10 MeV. The relative intensities of spectral lines depend on the oscillator strengths of the cascade transitions and the spectra exhibit irregular behavior. There occurs a gap between 210 eV and 650 eV where no emission lines appear. There may occur some emission around 520 eV from emission following the production of K shell vacancies in the projectile ions but the cross sections for collisions with H_2 are small.

The emission spectrum of oxygen ions in a given charge state is the sum of lines produced from all the populated excited states. Fig.14 shows the emission spectrum for lines of O^{+7} arising in the stopping of O^{+7} ions with an initial energy of 10 MeV. Many individual levels are populated, producing a spectrum remarkably similar to the Lyman series of O^{+7}. We calculated the emission spectra from other charge states using dynamical energy and charge distributions. Fig.15 shows the cascade spectrum from the O^{+6} charge state emitted in the complete stopping of projectiles with initial energy of 10 MeV.

Differences between the emission spectra of excited ions, populated due to electron captures, may help to identify the physical mechanism producing x-rays. Thus, electron captures by highly charged slow ions has been suggested as an important source of the x-ray radiation from comets [*Cravens* , 1997, *Mumma et al.*, 1997]. Slow electron

capture collisions populate selectively excited states about a specific level $I_b \sim I(n_q, l)$, where I_b is the ionization potential of the bath gas molecules. The resulting x-ray and EUV emission spectra will reflect the properties of the cascade spectra as depicted in Figs.12 and 13. These spectra, induced by the slowed highly stripped ions, differ in detail from the emission spectra of the fast ions in the Jovian aurora, presented in Figs.14 and 15. The charge abundance and population of the excited states of initially fast ions are regulated by the stopping process, while for slow ions they depend only on the initial charge state.

The total emission spectra of oxygen ions in Jovian auroras may be calculated from the dynamical energy and charge distributions $F(q, E, n)$ and the intensity and initial kinetic energy composition $f(E_{in})$ of the flux of precipitating oxygen ions. The sum of all cascade spectra emitted by different q-charge states is then integrated with respect to the initial energy distribution of precipitating ions $f(E_{in})$ which is known in the energy range from 5 MeV up to 160 MeV [*Gehrels and Stone* , 1983]. The global flux J_g of oxygen ions with these energies is about 10^{24} s^{-1}. The resulting cascade emission spectra are presented in Fig.16. The intensities of the x-ray and EUV spectral lines are given by the number of photons produced per second by the precipitating oxygen ions and are normalized to unit ion flux in particles per second. Multiplication of the normalized line intensities from Fig.16 with the global flux J_g gives the total intensities of spectral lines emitted by oxygen ions in the Jovian atmosphere.

Our calculations yield the energy input into specific emission lines. The total energy in the Lyman-like photons in Fig.15 with energies in excess of 650 eV is 10.8 keV, 0.1% of the initial 10 MeV. The energy input into the Lyman lines of O^{+7} increases with initial projectile energy to a value of 17.5 keV for an initial energy of 100 MeV and the conversion efficiency decreases uniformly to 0.02%. The accumulated power in the oxygen emission spectrum $P(E)$, shown in Fig.17, gives the energy flux of all photons with energies larger than E. The number of soft x-ray photons in the emission spectra is large because of the high abundances of low charge states and contributions from cascade transitions of high charge states though high energy lines carry a significant fraction of the total energy input. The luminosity L_O of the x-ray emission of oxygen ions with energy larger than 0.2 keV is calculated by multiplying the accumulated power $P(0.2\ keV)$ by the global flux $J_g = 10^{24}\ s^{-1}$: $L_O \simeq 4.1 * 10^9\ W$. This is equal to the estimated value of $4 * 10^9\ W$ for the total luminosity of oxygen and sulfur ions given by *Metzger et al.* (1983), but four times larger than the luminosity given by *Waite et al.* (1994). The value of the oxygen x-ray luminosity, calculated by *Cravens et al.* (1995), is an order of magnitude smaller, a difference that may result from the smaller conversion efficiency they used.

Detailed comparisons between calculated line intensities of the oxygen emission and

measured spectra are not possible due to the low spectral resolution of the x-ray detectors and their non-uniform spectral sensitivity [*Metzger et al.*, 1983, *Waite et al.*, 1994]. Instead we compare the calculated power function $P(E)$ with some overall characteristics of the measured spectra. The power of the emitted photons with energies from 100 eV to 200 eV is $9.9 * 10^8$ W and it accounts for 25% of the luminosity L_O of photons with energy larger than 200 eV. A similar value, varying between 30% and 40%, is obtained from the extrapolated power law spectra of *Metzger et al.* (1983). We have found that the number of photons increases significantly as the photon energies become less than 150 eV. We obtain for the luminosity of oxygen ion emission in the narrow spectral interval of $100 - 150$ keV $7.8 * 10^8$ W or 19% of L_o. The extrapolated power law spectra [*Metzger et al.*, 1983] give this fraction to be between 18% and 30%. Spectra of x-ray photons in the ROSAT observations [*Waite et al.*, 1994] and a theoretical evaluation of the count spectra for this experiment [*Cravens et al.*, 1995] show a sharp decrease in the detected photon flux for energies less than 200 eV attributable to a lack of sensitivity of the ROSAT instrument. The flux of photons with energies less than $150eV$ is enriched by cascade transitions from high charge ions as well as emission from the ions in medium and low charge states.

X-ray and EUV radiation from Jovian auroras or from comets provide a valuable diagnostic of the role of heavy ions. The relative intensities of spectral lines at improved resolution could be employed to determine the identity and energy of the precipitating ions. In Fig.18 the accumulated number of photons, emitted by precipitating oxygen ions, is compared with the power law fitting of x-ray spectra detected from Jovian auroras [*Metzger et al.*, 1983] and comet Hale-Bopp [*Owens et al.*, 1998]. The spectra are normalized at the photon energy of 200 eV, where the maximum count rates of the x-ray detectors occur [*Waite et al.*, 1994, *Owens et al.*, 1998]. The x-ray spectrum from the auroras exhibits a larger fraction of high energy photons than the cometary emission because of repeated stripping and electron capture collisions of the precipitating energetic ions. The fraction of high energy photons in cometary x-ray emission decreases more rapidly, because these photons can be produced by heavy ions [*Cravens*, 1997, *Mumma et al.*, 1994] only at the beginning of the stopping process . The kinetic energies of solar wind ions are not enough to maintain a significant abundance of high charge ions as they propagate in the cometary atmosphere.

The spectrum of x-ray emission in the Jovian aurora depends on the chemical composition of the ionospheric fluxes. Precipitating sulfur ions will produce a spectrum distinct from that of the oxygen ions [*Waite et al.*, 1994]. The gap in the emission spectra between 210 eV and 560 eV, shown in the Fig.16, reflects excitation spectra of oxygen projectiles only and some spectral lines of sulfur ions may appear in this energy interval.

References

Cocke C.L. and E. C. Montenegro, Ionization by the electron-electron interaction in ion-atom collisions, *Comments At. Mol. Phys., 32*, 131 , 1996.

Cravens T. E., E. Howell, J. H. Waite Jr., and G. R. Gladstone, Auroral oxygen precipitation at Jupiter, *J. Geophys. Res., 100*, 17153, 1995.

Cravens T. E., Comet Hyakutake x-ray source: Charge transfer of solar wind heavy ions,*Geophys. Res. Lett., 24*, 105 , 1997.

Gehrels N., E. C. Stone, Energetic oxygen and sulfur ions in the Jovian magnetosphere and their contribution to the auroral excitation, *J. Geophys. Res., 88*, 5537 , 1983.

Green, L. C., R. P. Rush, C. D. Chandler, Oscillator strengths and matrix elements for the electric dipole moment for hydrogen, *Astrophys. J. Suppl., 3*, 37, 1957.

Greenland P. T., Electron Capture by Highly stripped ions, *Physics Repots, 81*, 131, 1982.

Hoang-Bihn D., An exact calculation of hydrogen radial integrals and oscillator strengths for principal numbers up to $n \approx 1000$, *Astron. Astrophys., 238*, 449 , 1990.

Horanyi M., T. E. Cravens, J. H. Waite, Jr., The precipitation of energetic heavy ions into the upper atmosphere of Jupiter, *J. Geophys. res., 93*, 7251, 1988.

Janev R. K. and H. Winter, State-selective electron capture in atom-highly charges ion collisions, *Phys. Lett., 117*, 265 , 1985.

Metzger, A. E., D. A. Gilman, J. L. Luthey, K. C. Hurley, H. W. Schnopper, F. D. Seward and J. D. Sullivan, The detection of X rays from Jupiter, *J. Geophys. Res., 88*, 7731 - 7741, 1983.

Montenegro E. C. and W. E. Meyerhof, Sum rules and electron-electron interaction in two-center scattering, *Phys. Rev. A., 43*, 2289, 1991.

Montenegro E. C., G. M. Sigaud and W. E. Meyerhof, Intermediate-velocity atomic collisions. V. Electron capture and loss in C^{3+} and O^{5+} collisions with H_2 and He , *Phys. Rev. A., 45*, 1575 , 1992 .

Lisse C. M., K. Dennerl, J. Englhauser, M. Harden, F. E. Marshall, M. J. Mumma, R. Petre, J. P. Pye, M. J. Ricketts, J. Schmitt, J. Trümper, and R. G. West, Discovery of X-ray and extreme ultraviolet emission from comet C/Hyakutake 1996 B2, *Science, 274*, 205, 1996.

Mumma M. J., V. A. Krasnopolsky and M. J. Abbott, Soft x-rays from four comets observed with EUVE, *ApJ, 491*, L125, 1997.

Owens A., A. N. Parmar, T. Oosterbroek, A. Orr, L. A. Antonelli, F. Fiore, R. Schulz, G. P. Tozzi, M. C. Maccarone and L. Piro, Evidence for the dust-related x-ray emission from comet C/1995 O1 (Hale-Bopp), *ApJ, 491*, L125, 1998.

Phaneuf R. A., R. K. Janev, and M. S. Pindzola, Collisions of carbon and oxygen ions with electrons, H, H_2 and He, *Rep. ORNL-6090/V5*, US Department of Energy, Washinton, D. C., 1987.

Rees M. H., *Physics and Chemistry of the Upper Atmosphere*, Cambridge University Press, 1989.

Rost J. M. and T. Pattard, Analytical parameterization of the shape of atomic ionization cross section, *Phys. Rev. A, 55*, R5, 1997.

Ryufuku H. and T. Watanabe, Total and partial cross sections for charge transfer in collisions of multi-charged ions with atomic hydrogen, *Phys. Rev. A., 20*, 1828, 1979.

Sobelman I. I., Atomic Spectra and Radiative Transitions, *Springer-Verlag*, Berlin, 1979.

Striganov A. R. and N. S. Sventitskii, Tables of spectral lines of neutral and ionized atoms, *Plenum , New York,* 1968.

Wiese W. L., J. R. Fuhr and T. M. Deters, Atomic transition probabilities of carbon, nitrogen, and oxygen, *J. Phys. Chem. Ref. Data, Monograph 7*, NIST, 1996.

Waite, J. H. Jr., F. Bagenal, F. Seward, C. Na, G. R. Gladstone, T.E. Cravens, K. C. Hurley, J. T. Clarke, R. Elsner, and S. A. Stem, ROSAT observations of the Jupiter Aurora, *J. Geophys. Res., 99*, 14, 799, 1994.

Figure 1: Cross-sections of different inelastic channels in $O^{+5} + H_2$ collisions as functions of a kinetic energy. Curve 1 shows the charge transfer cross-section, 2 - the stripping cross-section, 3 - the cross-section for target ionization, and 4 - the total cross section.

Figure 2: Probabilities of various charge-changing processes in $O^{+5} + H_2$ collisions as functions of the kinetic energy of oxygen ions. Curve 1 shows the probability p_- of the electron capture, 2- the probability of stripping p_+, 3- the probability of the target ionization p_0 .

Figure 3: Dynamical energy and charge distributions in an ensemble of initially mono-energetic oxygen ions with $E_{in} = 10\ MeV$ and $q_{in} = 1$ after $n = 2 * 10^3,\ 10^4,\ 2 * 10^4, 3 * 10^4, 5 * 10^4, 10^5$ and $1.5 * 10^5$ collisions.

Figure 4: Energy and charge distribution function $F(q, E, n)$ for the ensemble of 1000 oxygen ions after $2 * 10^5$ collisions. All ions have started a stopping process with the equal initial energies $E_{in} = 20\ MeV$ and charges $q_{in} = 1$.

Figure 5: Average energy $E_{av}(n)$ and average charge $q_{av}(n)$ for the dynamical distribution of oxygen ions as functions of the number of collisions n. The initial energy of the ions is $E_{in} = 20\ MeV$ and the initial charge is $q_{in} = 1$.

Figure 6: Phase trajectories of the central point $\{E_{av}(n), q_{av}(n)\}$ of the energy and charge distribution for the stopping of oxygen ions with initial parameters $E_{in} = 10\ MeV$, $q_{in} = 3, 8$ (solid curves) and with $E_{in} = 20\ MeV, q_{in} = 1$ (the dashed curve). Dotted curves shows the central point trajectory for the equilibrium charge distribution model.

Figure 7: Abundance of the different charge states in an ensemble of 1000 ions as a function of the number of collisions. The initial energy is $10\ MeV$, the initial ion charge is $q_{in} = 3$ in Fig.7a and $q_{in} = 8$ in Fig.7b.

Figure 8: Dynamical (solid curves) and equilibrium (dashed) charge distributions in a 1000 particle flux of precipitating oxygen ions . Number of collisions from the beginning of the stopping process is shown along with the distribution curves. Initial parameters of oxygen ion flux are $E_{in} = 10\ MeV, q_{in} = 1$.

Figure 9: Number of resonant x-ray photons emitted by a single oxygen projectile from different charge states after n collisions. The energies of resonant photons are larger than 653 eV for the $q = 7$ charge state , 560 eV for $q = 6$, and 79 eV for $q = 5$. Dashed curve shows the ion average energy $E_{av}(n)$ in MeV.

Figure 10: Quantum yield of the oxygen projectile emission from different charge states $q = 5, 6$ and 7 as functions of the mean energy $E_{av}(n)$. The ion initial energy is 10 MeV.

Figure 11: The same as in Fig.10 for an oxygen ion with initial energy of 100 MeV.

Figure 12: Cascade emission spectra produced by the excited states of a hydrogen-like ion $O^{+7}(n_q)$ with the quantum number $n_q = 5$. Initial energy is $E_n = 10$ MeV.

Figure 13: The same as in Fig.12 for the quantum number $n_q = 8$.

Figure 14: Cascade spectrum induced by a hydrogen-like ion O^{+7} from the set of excited states populated in charge-capture collisions. Initial ion energy is $E_{in} = 10$ MeV.

Figure 15: The same as in Fig.14 for the ion charge state O^{+6}.

Figure 16: Total spectra of x-ray and EUV photons emitted by oxygen ions precipitating in the Jupiter atmosphere. Number of photons normalized to the unit flux of precipitating ions.

Figure 17: Accumulated energy input into the different lines of the oxygen emission spectrum. Value of the energy input is normalized to the unit flux of precipitating oxygen ions.

Figure 18: Accumulated number of the EUV and x-ray photons in energy interval from 80 eV to 1 keV . Solid curves is the power fitting of observed x-ray spectra from Jovian auroras. Dashed line is the power spectra of x-ray emission from Hale-Bopp comet.

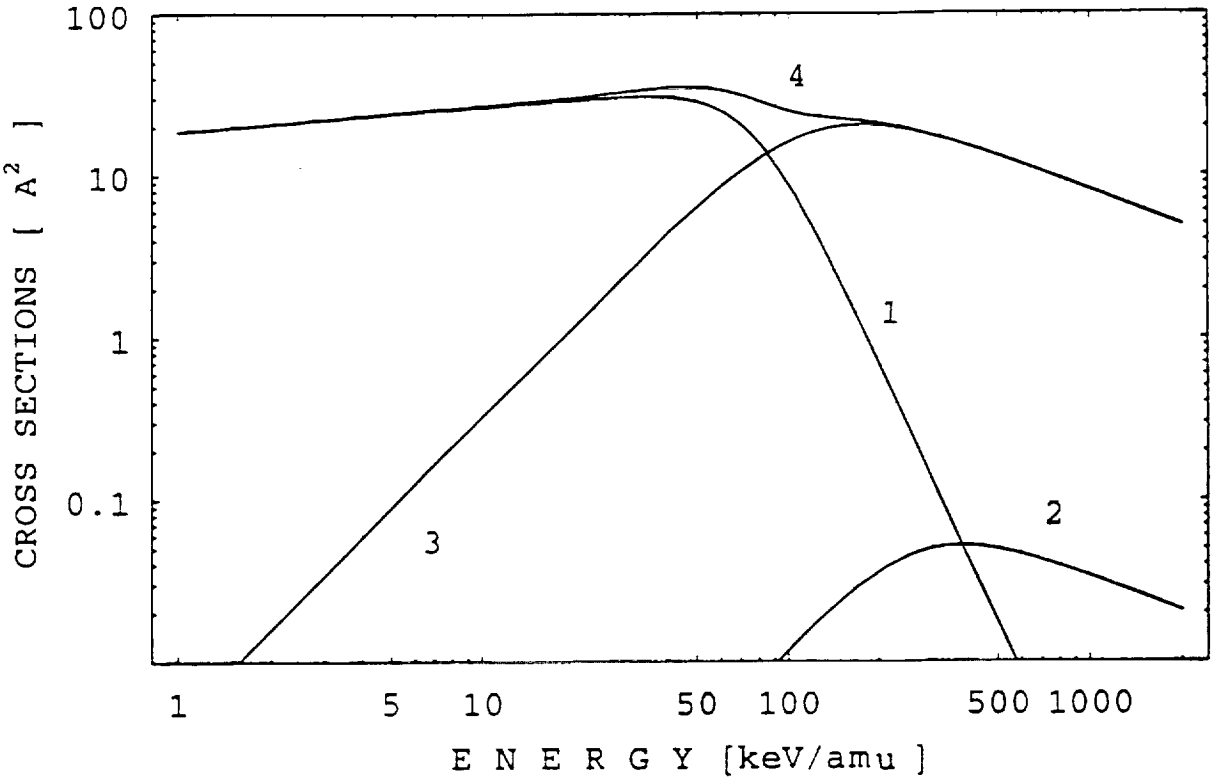
100
10
1
0.1
CROSS SECTIONS [A^2]
4
1
2
3
1
5
10
50
100
500
1000
E N E R G Y [keV/amu]

Fig 1

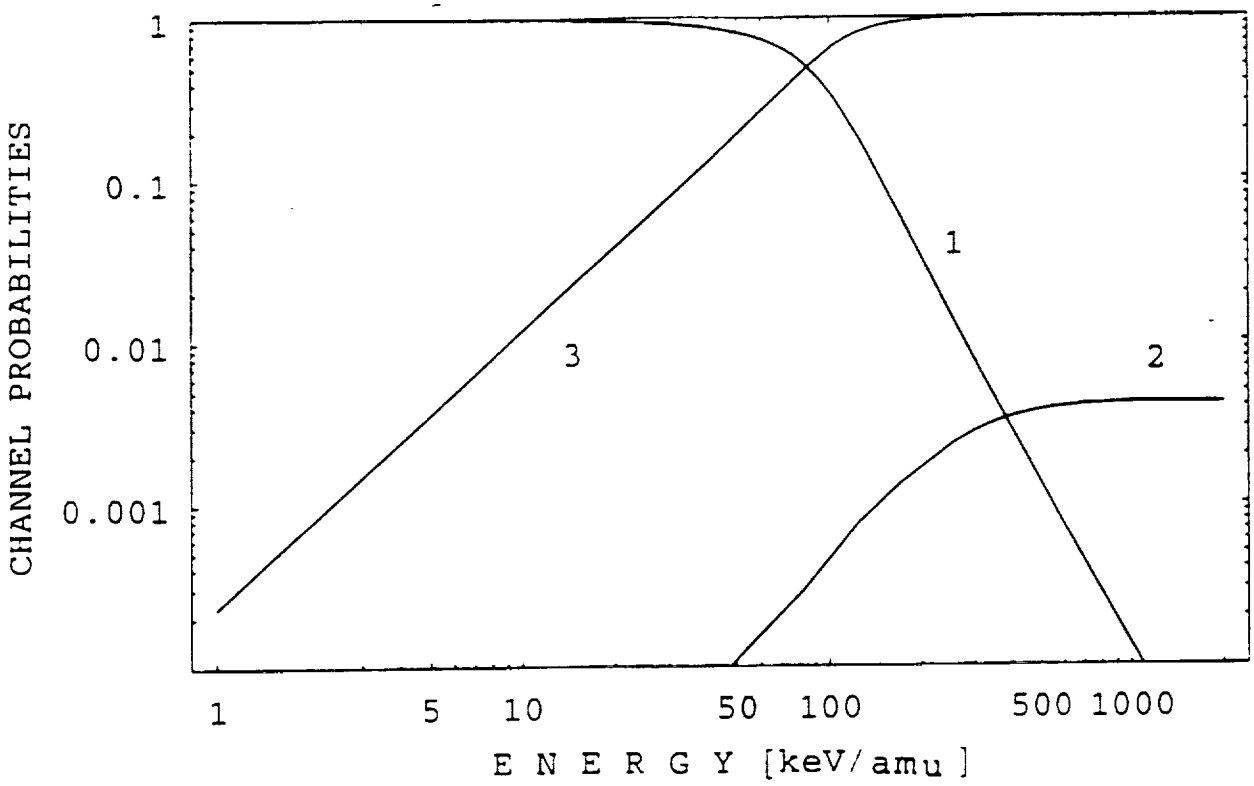
CHANNEL PROBABILITIES
1
0.1
0.01
0.001
1
5
10
50
100
500
1000
E N E R G Y [keV/amu]
1
2
3

Fig. 2

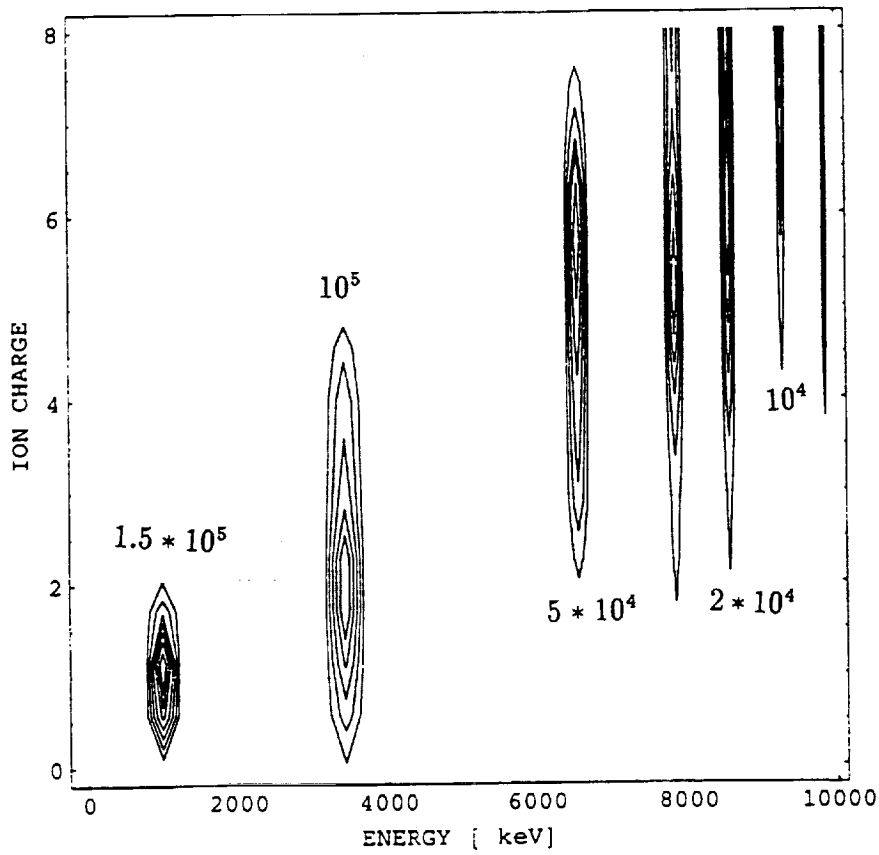
8
6
4
2
0
ION CHARGE
0
2000
4000
6000
8000
10000
ENERGY [keV]
1.5 * 10^5
10^5
5 * 10^4
2 * 10^4
10^4

Fig.3

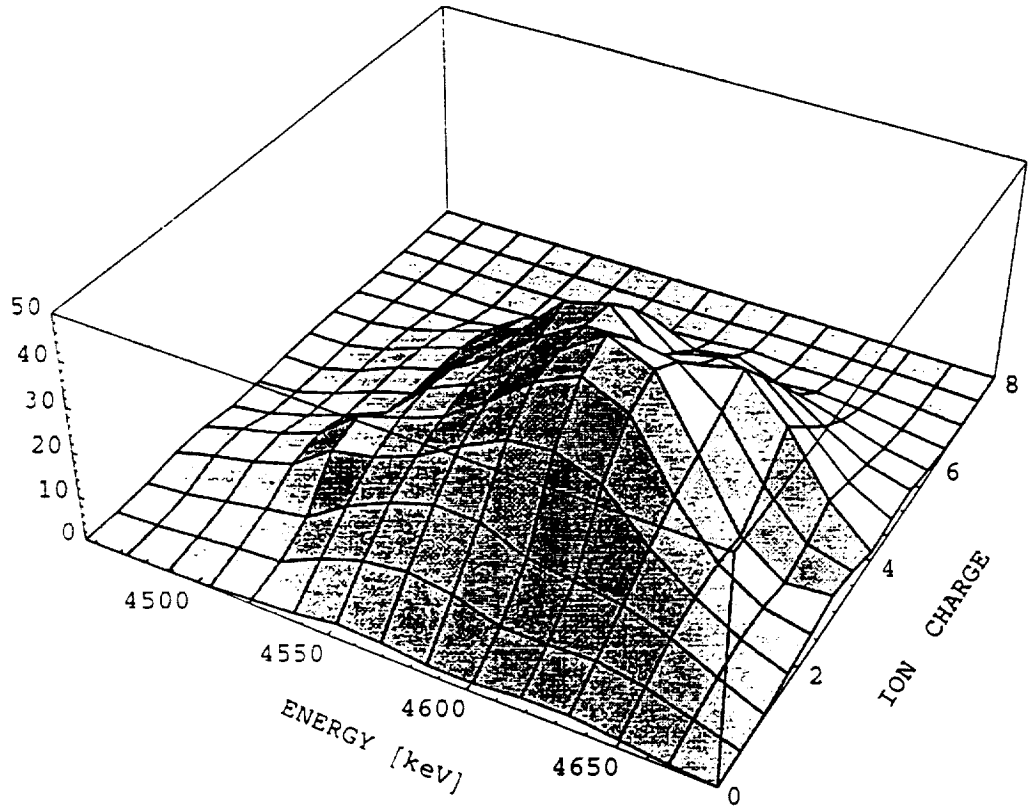
50
40
30
20
10
0
4500
4550
4600
4650
ENERGY [keV]
0
2
4
6
8
ION CHARGE

Fig.4

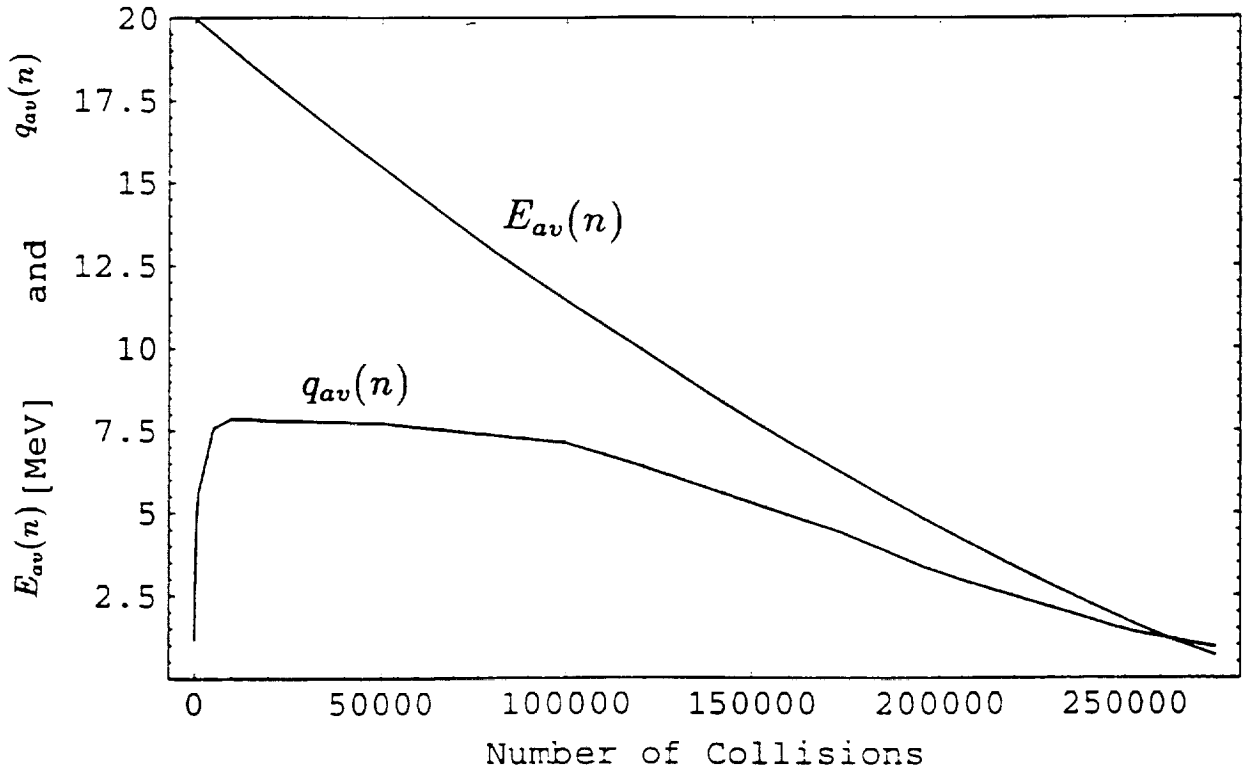
20
17.5
15
12.5
10
7.5
5
2.5
$E_{av}(n)$ [MeV] and $q_{av}(n)$
$E_{av}(n)$
$q_{av}(n)$
0
50000
100000
150000
200000
250000
Number of Collisions

Fig.5

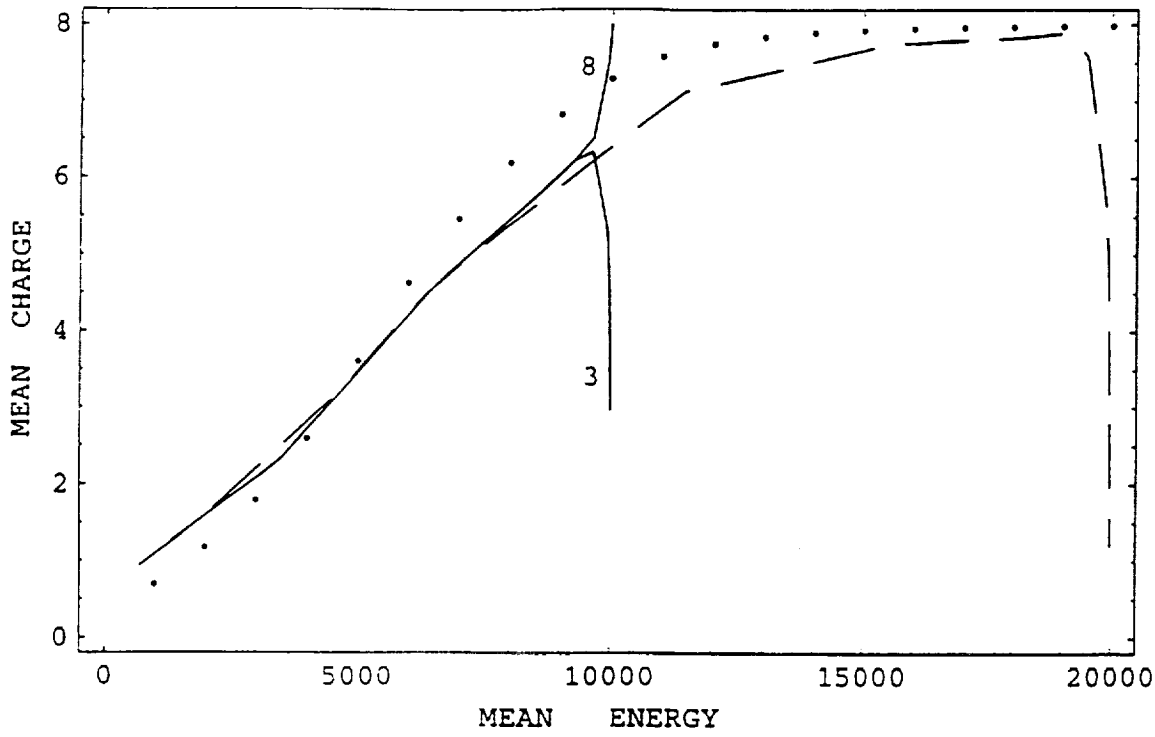

Fig 6

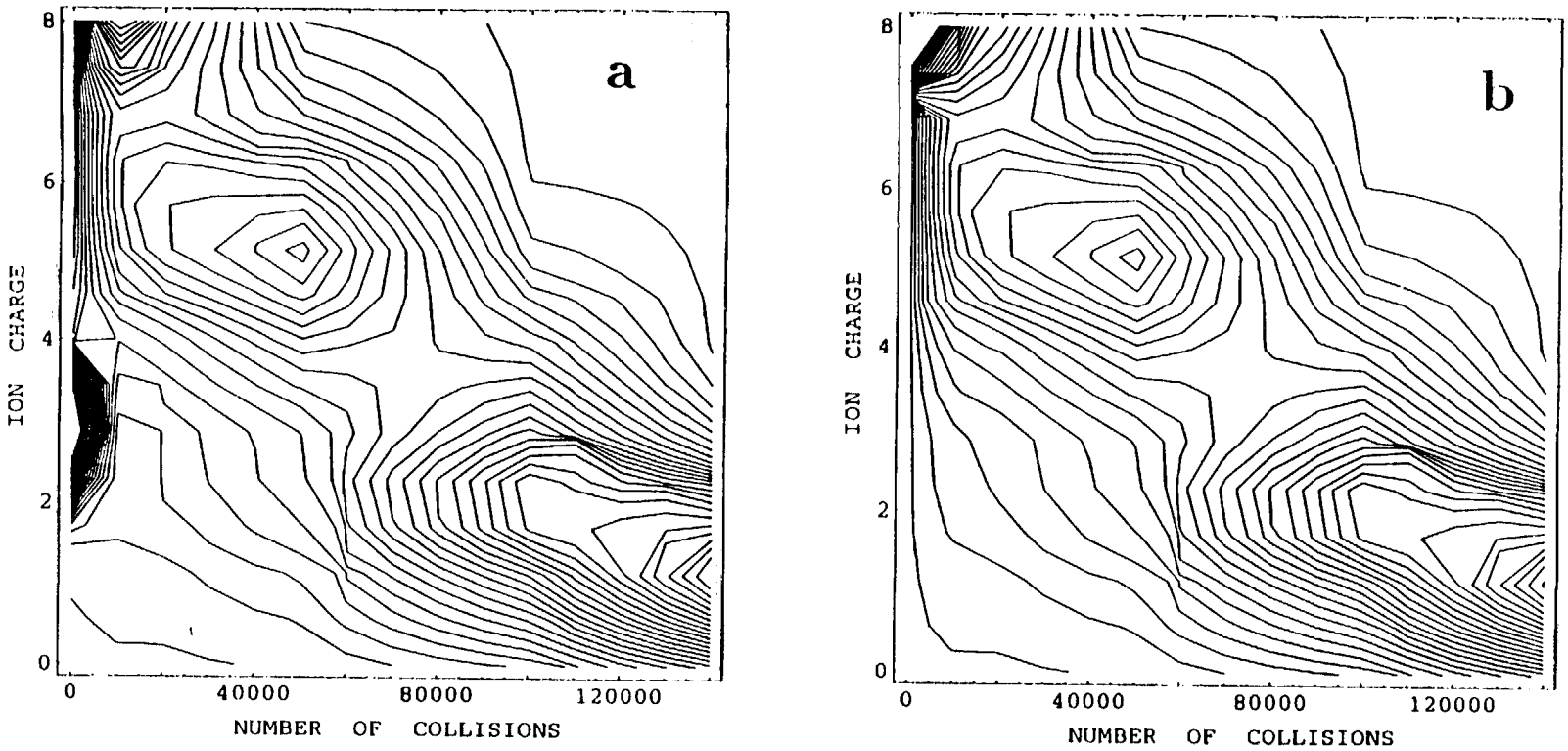
a
b
ION CHARGE
NUMBER OF COLLISIONS
0
2
4
6
8
0
40000
80000
120000

Fig.7

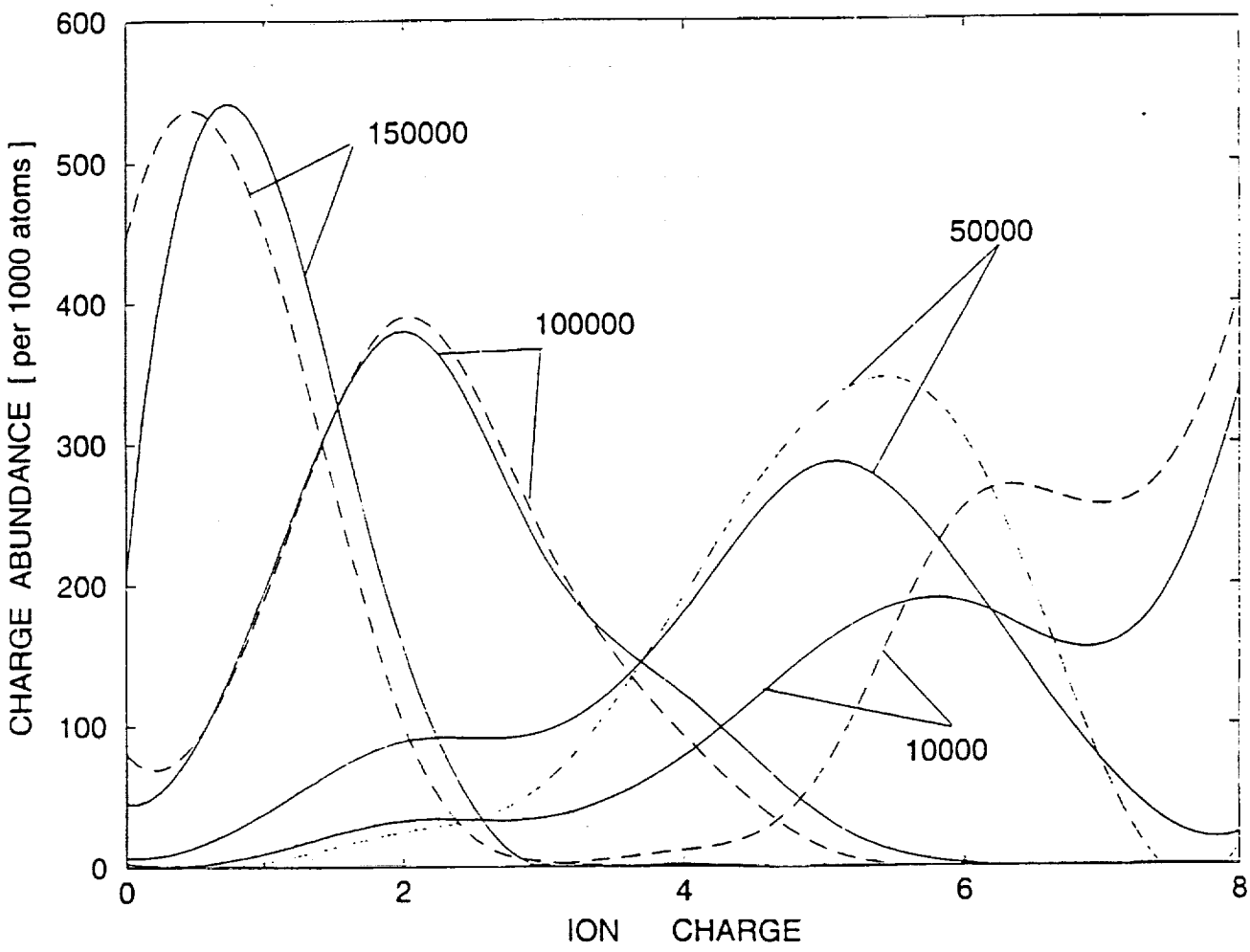
600
500
400
300
200
100
0
CHARGE ABUNDANCE [per 1000 atoms]
150000
100000
50000
10000
0
2
4
6
8
ION CHARGE

Fig.8

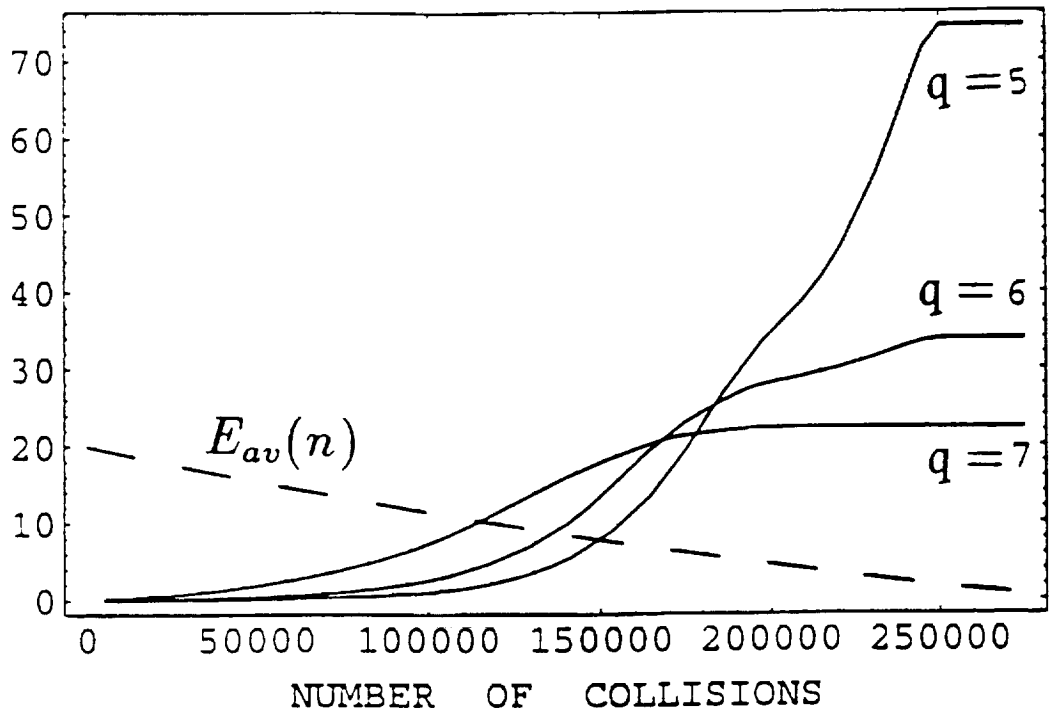
70
60
50
40
30
20
10
0
0
50000
100000
150000
200000
250000
NUMBER OF COLLISIONS
$E_{av}(n)$
q = 5
q = 6
q = 7

Fig.9

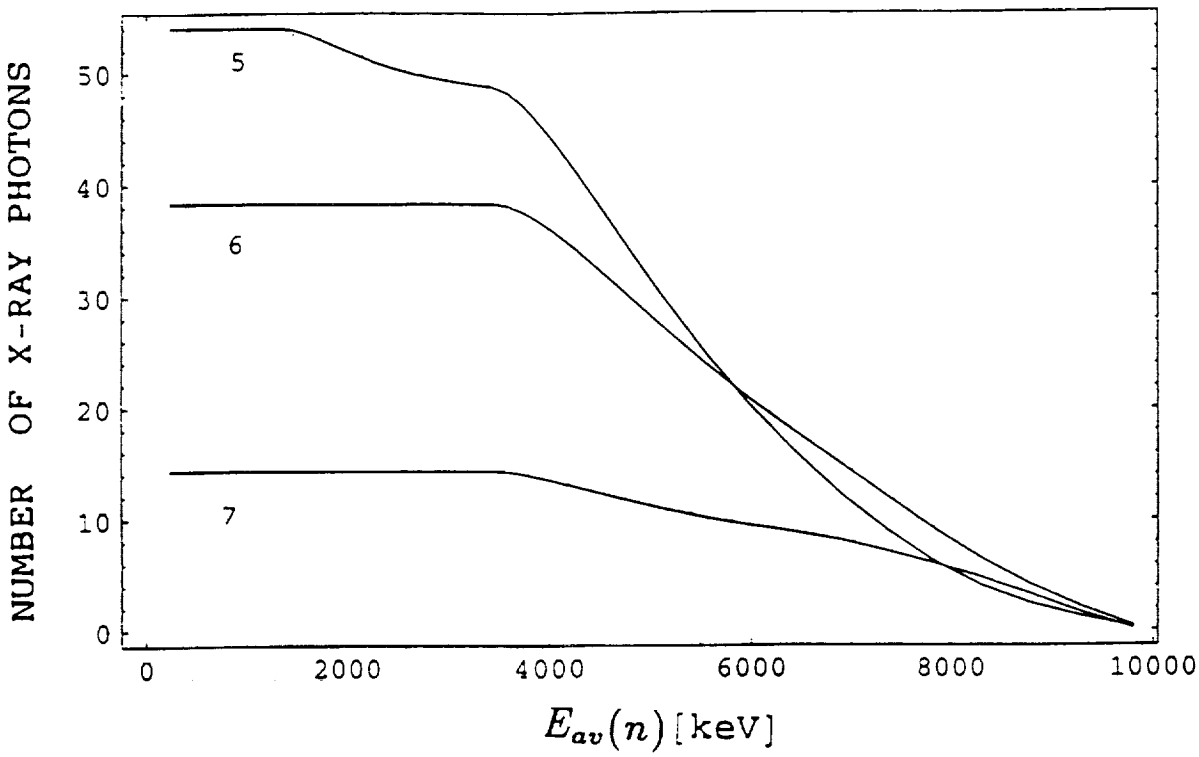
NUMBER OF X-RAY PHOTONS
0
10
20
30
40
50
5
6
7
0
2000
4000
6000
8000
10000
$E_{av}(n)$ [keV]

Fig.10

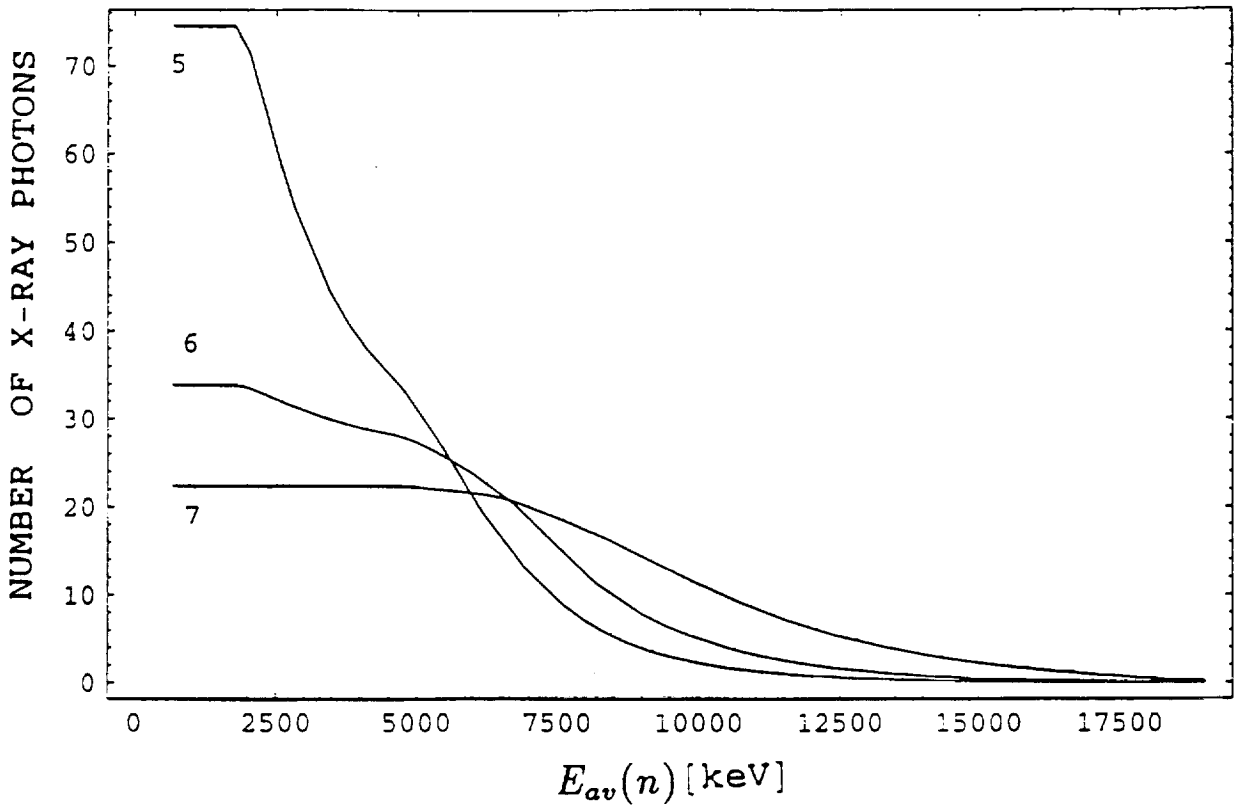
NUMBER OF X-RAY PHOTONS
70
60
50
40
30
20
10
0
5
6
7
0
2500
5000
7500
10000
12500
15000
17500
$E_{av}(n)$ [keV]

Fig.11

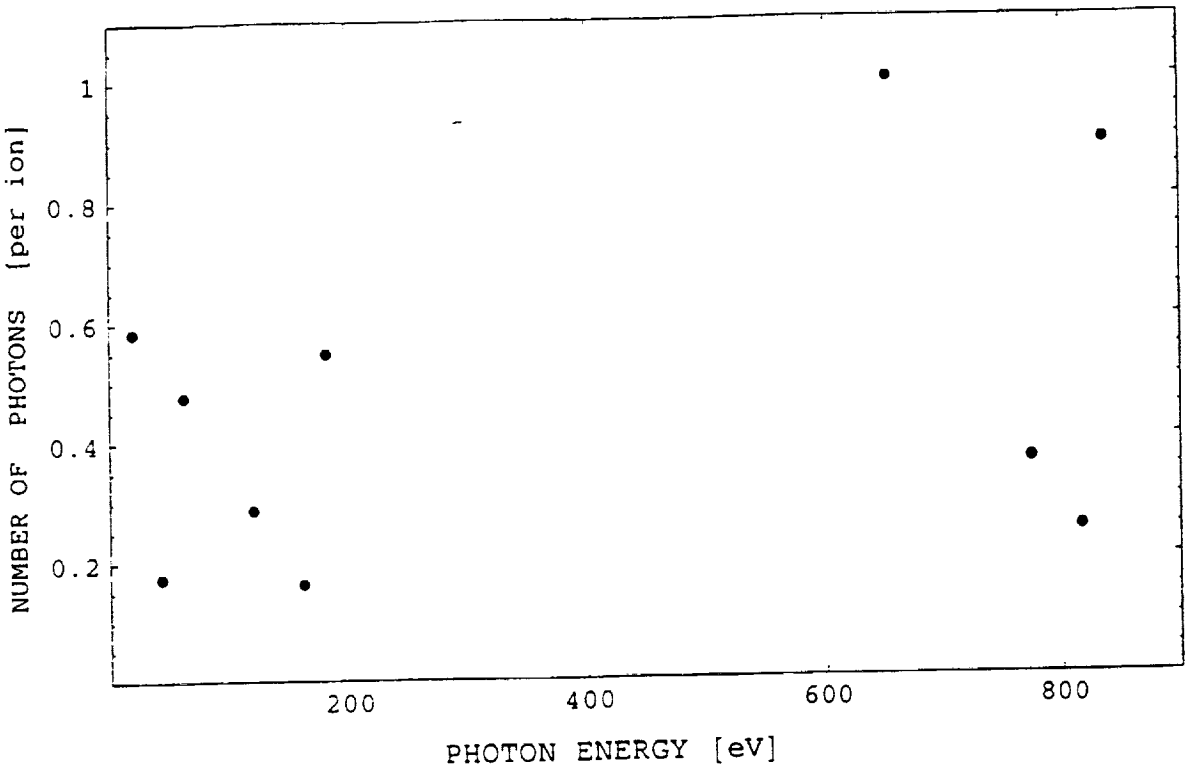
NUMBER OF PHOTONS [per ion]
1
0.8
0.6
0.4
0.2
200
400
600
800
PHOTON ENERGY [eV]

Fig.12

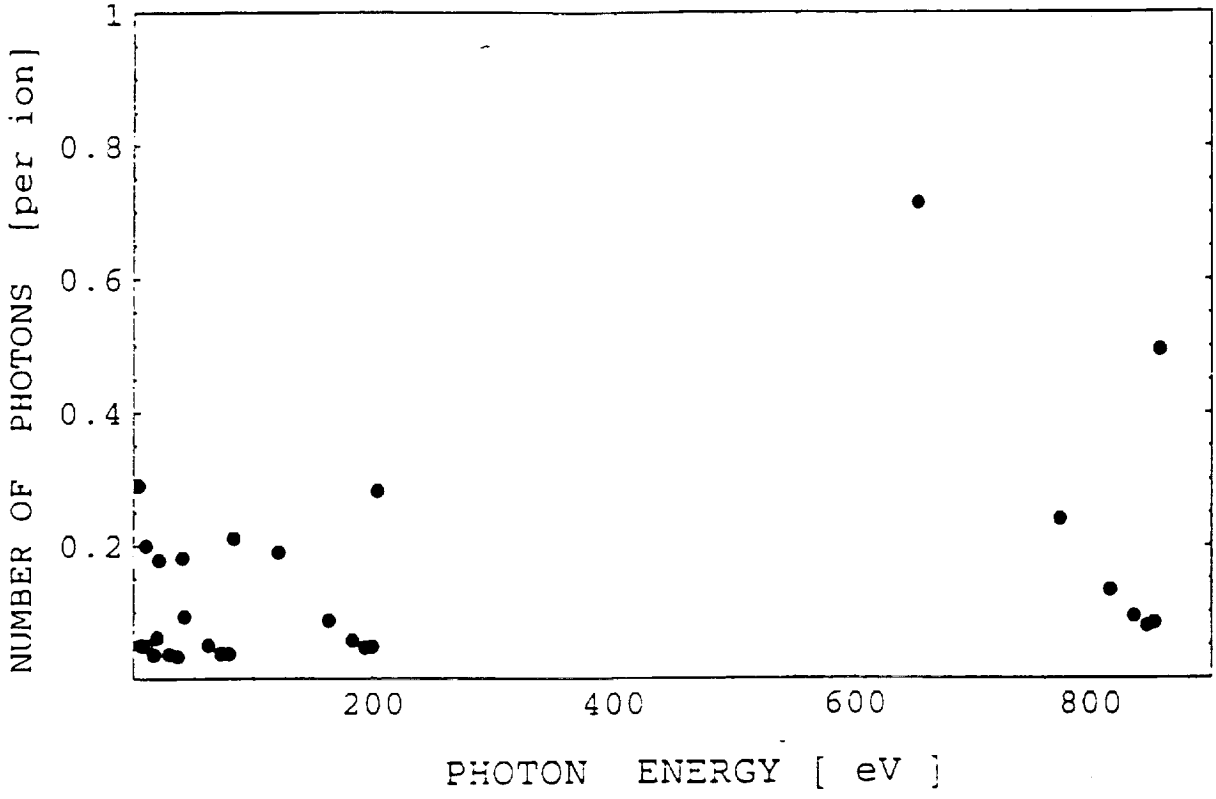
NUMBER OF PHOTONS [per ion]
1
0.8
0.6
0.4
0.2
200
400
600
800
PHOTON ENERGY [eV]

Fig.13

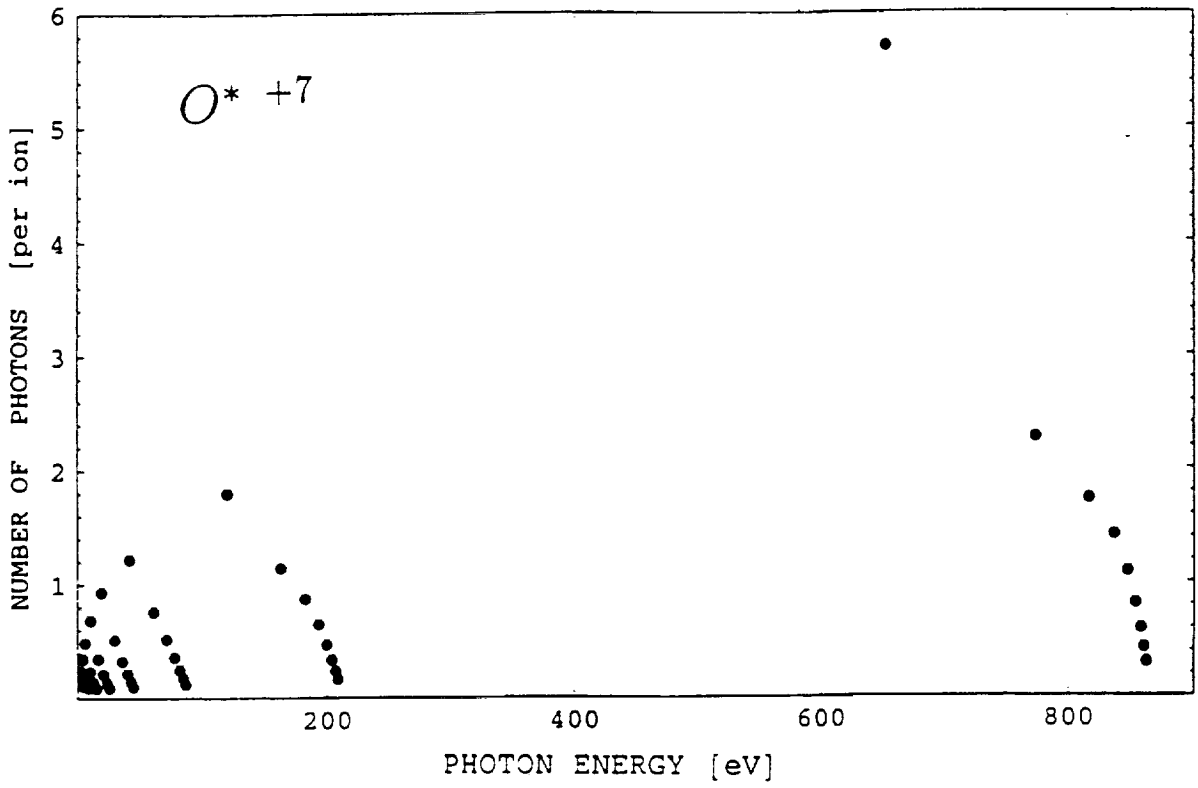
O* +7
NUMBER OF PHOTONS [per ion]
PHOTON ENERGY [eV]
1
2
3
4
5
6
200
400
600
800

Fig.14

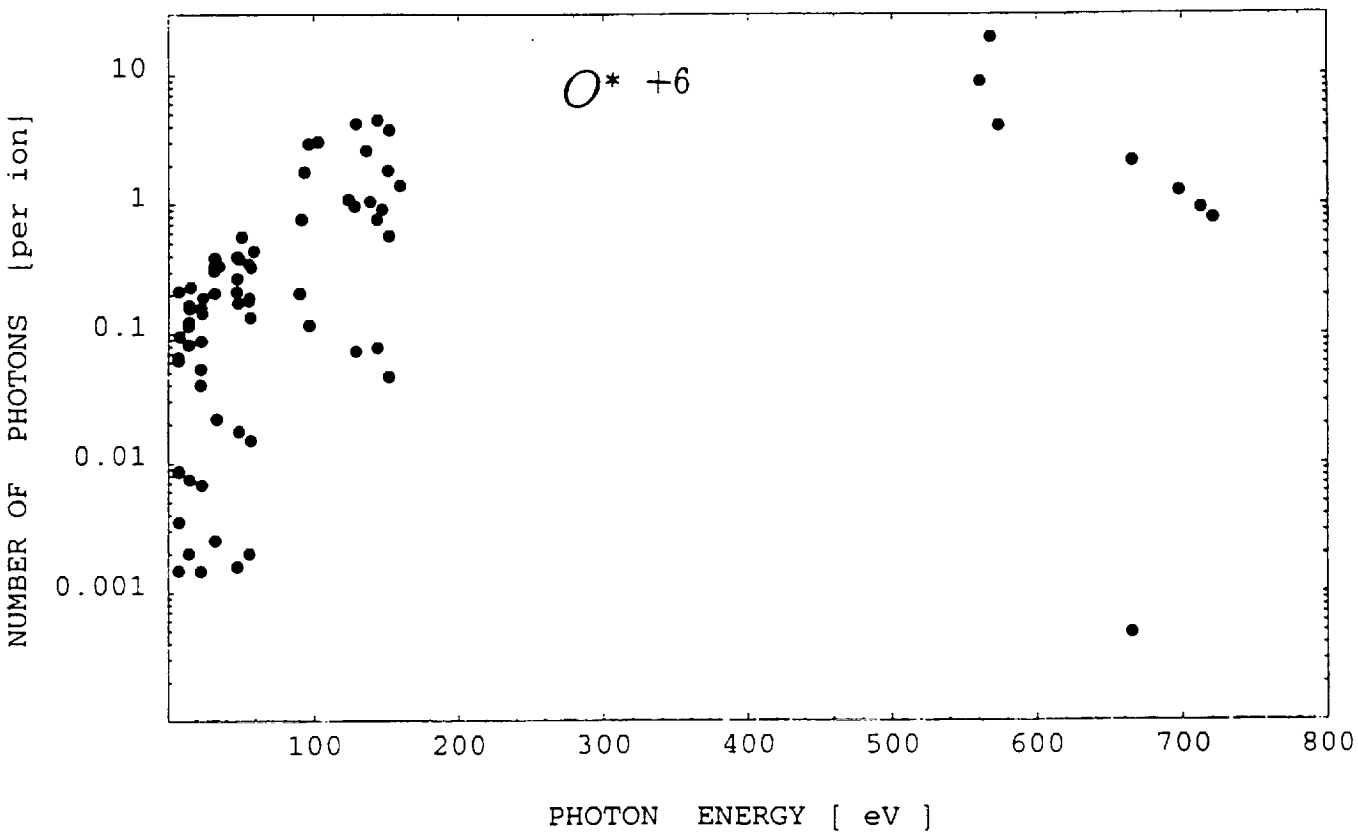
O* +6
10
1
0.1
0.01
0.001
NUMBER OF PHOTONS [per ion]
100
200
300
400
500
600
700
800
PHOTON ENERGY [eV]

Fig 15

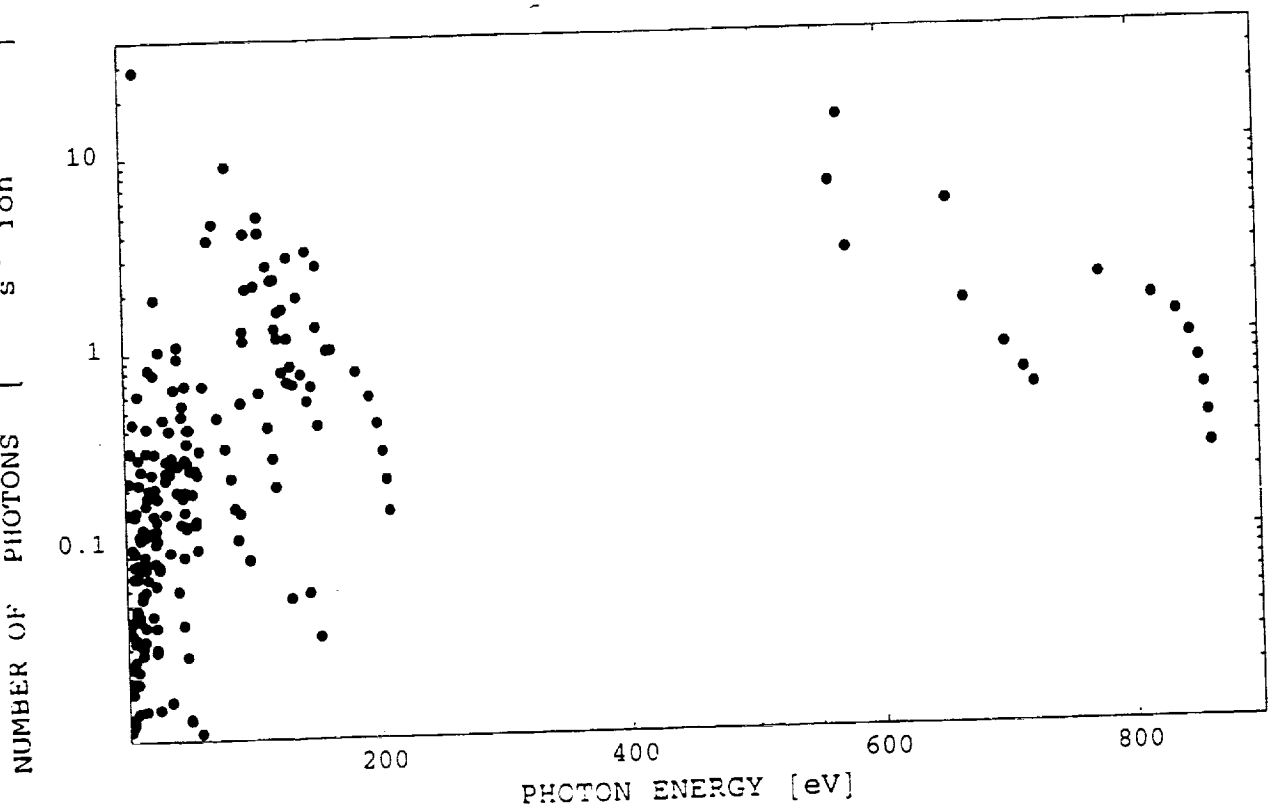
NUMBER OF PHOTONS [s⁻¹ ion⁻¹]
10
1
0.1
200
400
600
800
PHOTON ENERGY [eV]

Fig.16

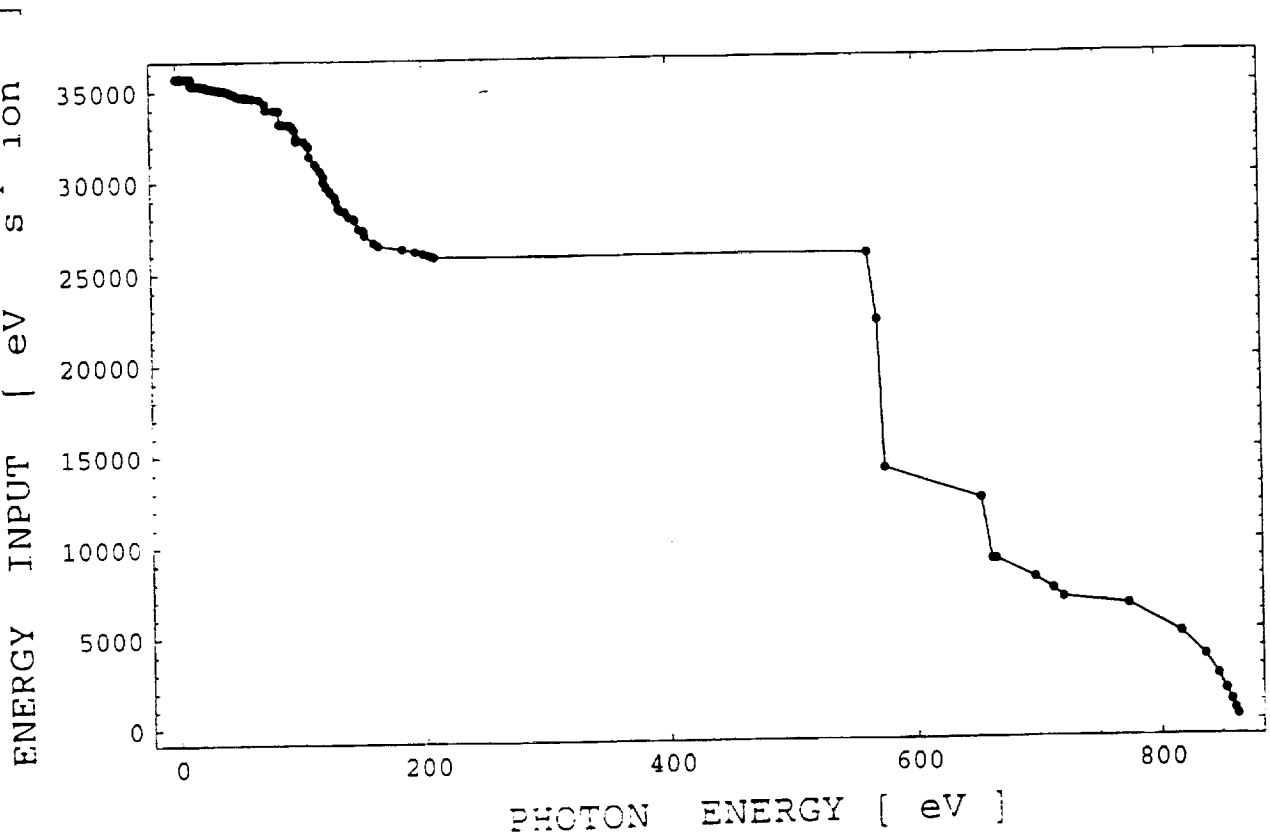
ENERGY INPUT [eV s^{-1} ion^{-1}]
35000
30000
25000
20000
15000
10000
5000
0
0
200
400
600
800
PHOTON ENERGY [eV]

Fig.17

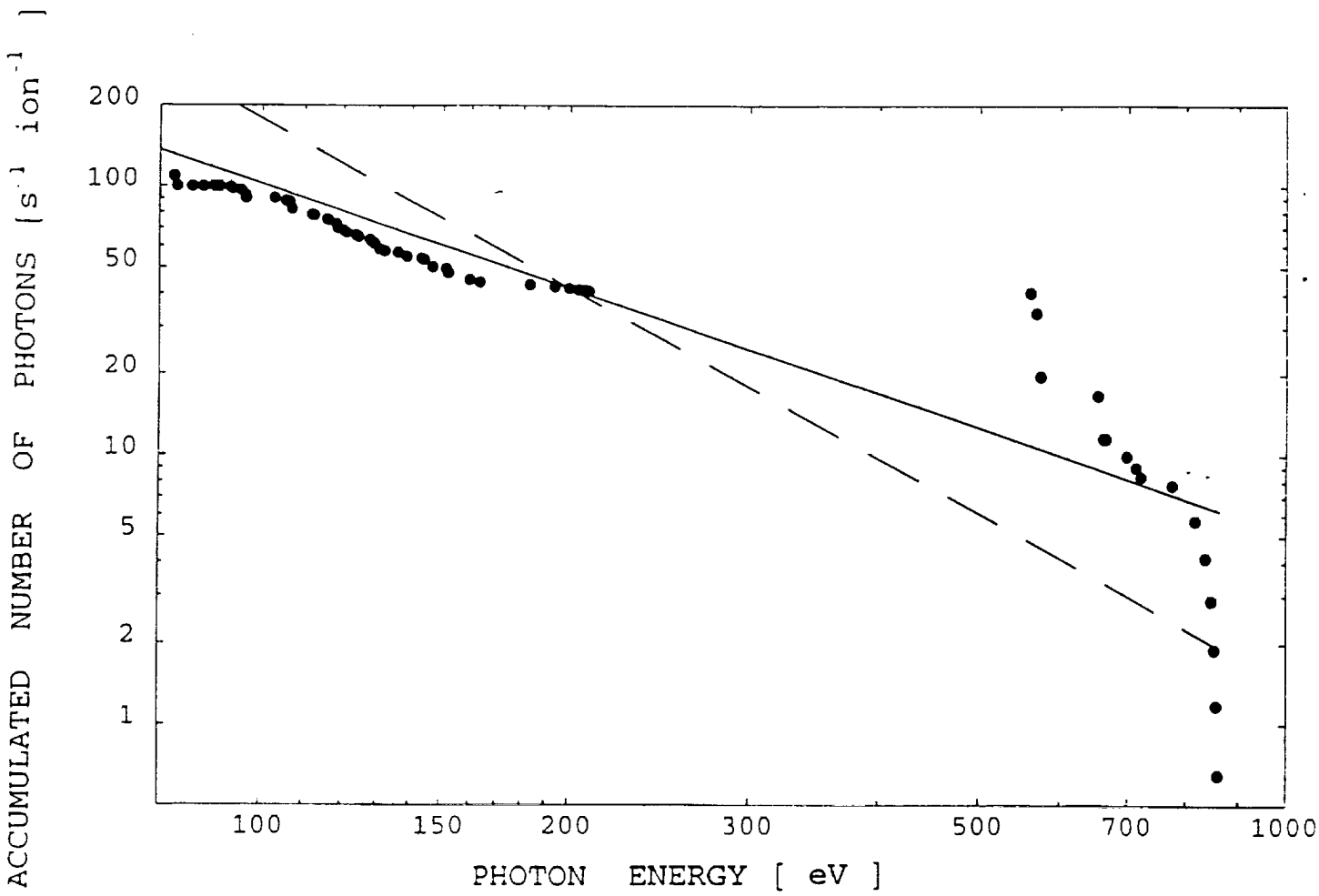
ACCUMULATED NUMBER OF PHOTONS [s⁻¹ ion⁻¹]
200
100
50
20
10
5
2
1
100
150
200
300
500
700
1000
PHOTON ENERGY [eV]

Fig.18